Verification of wave turbulence theory in the kinetic limit

Alexander Hrabski [*] and Yulin Pan [†]
Department of Naval Architecture and Marine Engineering, University of Michigan, Ann Arbor, Michigan 48109, USA

(Received 16 January 2024; accepted 1 May 2024; published 20 May 2024)

Using the 1D Majda-McLaughlin-Tabak model as an example, we develop numerical experiments to study the validity of the wave kinetic equation (WKE) at the kinetic limit (i.e., small nonlinearity and large domain). We show that the dynamics converge to the WKE prediction, in terms of the closure model and energy flux, when the kinetic limit is approached. When the kinetic limit is combined with a process of widening the inertial range, the theoretical Kolmogorov constant can be recovered numerically to a very high precision.

DOI: 10.1103/PhysRevResearch.6.023184

I. INTRODUCTION

Wave turbulence (WT) describes the out-of-equilibrium statistical dynamics of multiscale wave systems. The theory of WT has been successfully applied to various physical contexts, including ocean surface waves [1,2], internal gravity waves [3,4], quantum turbulence [5], and gravitational waves in the early universe [6]. For a given system, a statistical closure model can be developed that connects the high-order correlators of the wave field to pair correlators. When the closure model is taken in the kinetic limit, i.e., infinitesimal wave amplitude in an infinite domain, a wave kinetic equation (WKE) can be derived which describes the spectral evolution via a Boltzmann-like collision integral over wave-wave interactions.

One of the most important features of the WKE is that it yields stationary power-law solutions with constant flux, known as Kolmogorov-Zakharov (KZ) spectra. For direct cascades, the general form of the KZ solution of the wave action spectrum can be written as $n_k = CP^\alpha k^\gamma$, where k is the wave number, P is the energy flux, and $\alpha = 1/2$ and $\alpha = 1/3$ for systems with three- and four-wave resonances, respectively. C and γ are constants that can be calculated as a part of this solution. Attempts to verify the KZ solution heavily focus on the scaling exponent γ [7–10], with only a handful of them targeting the Kolmogorov constant C. Among the latter, recent experimental validations [e.g., 11,12] lead to larger discrepancies with theory (as much as a factor of 20 difference), partly due to the challenge of precisely measuring P from experimental data. The studies that are relatively successful consider well-controlled numerical simulations, including turbulence of capillary waves [13–15] and Bose-Einstein condensates [16], which provide values of C respectively about 40% above and 10% below the corresponding theoretical values. These two results signify that for a given power-law spectrum with theoretical slope γ, the energy flux computed from simulations are respectively about 0.5 and 1.3 [$\approx (1/1.40)^2$, 1.1^3] times of that from the KZ solution.

The scarce and limited success in verifying the Kolmogorov constant indicates an insufficient understanding of the validity of the WKE for stationary WT. This issue is more subtle than verification of WKE at an evolving state (e.g., [17]), where spectral evolution serves as a natural measure of success. We are mainly interested in two fundamental questions in this work: (1) What are the major obstacles in obtaining the theoretical value of C in simulations of dynamical equations? In particular, what does it take to bring the numerical value of C closer to the theoretical value than in previous validations? (2) How is the KZ spectrum (and more generally, the WT closure) realized in one-dimensional (1D) systems? We note that 1D WT is in a sense more difficult to describe than in higher dimensions [16–18] due to far fewer interactions for any given spectral range. One example of a 1D system is the Majda-McLaughlin-Tabak (MMT) model [7], for which the theoretical value of γ has been notoriously difficult to reproduce numerically for more than 20 years. This puzzle was resolved only recently in [9], where it was shown that the theoretical value of γ can be recovered with a much wider inertial range than those in previous studies. The Kolmogorov constant for this 1D system, on the other hand, has never been numerically studied.

With the two above questions in mind, we perform a numerical study of the MMT model focusing on the Kolmogorov constant in the stationary state. One feature distinguishing our current study from all previous studies is that we numerically probe the kinetic limit, by weakening nonlinearity while making the domain large. We show that the theoretical value of C can be recovered as a result of two limiting processes: (1) as we approach the kinetic limit, the dynamics of the MMT model converge to the WKE description, evaluated through the closure model and energy flux; (2) as we enlarge the inertial range, the value of C computed from the collision integral converges to the theoretical value to very high precision. In

[*] ahrabski@umich.edu
[†] yulinpan@umich.edu

component (1), we find that quasiresonances can lead to a difference between the MMT simulation and WKE prediction when the former is taken outside the kinetic limit as in [16]. In component (2), we find that an inertial range of at least 3.5 decades is needed for the convergence of C.

II. THE MMT MODEL AND KZ SOLUTION

The MMT model is a family of nonlinear dispersive equations for a complex field $\psi(x) = \psi \in \mathbb{C}$ that are widely used in the study of WT [7,19–21]. This model's popularity is in part due to its relatively simple structure, which reproduces many of the essential features of WT. Thus, it has been and remains a test bed for wave turbulence theory, as many conclusions drawn with this system are applicable broadly in wave turbulence. The MMT equation of interest to this work reads

$$i\frac{\partial \psi}{\partial t} = |\partial_x|^{1/2}\psi + |\psi|^2\psi, \tag{1}$$

where the derivative operator $|\partial_x|^{1/2}$ produces a dispersion relation $\omega_k = |k|^{1/2}$, the same as surface gravity waves. We consider the MMT equation on a 1D periodic domain of length L, where we have $\psi(t) = \sum_{k\in\Lambda_L} \hat{\psi}_k(t)e^{ikx}$, with $\Lambda_L \equiv 2\pi\mathbb{Z}/L$.

The statistical description of (1) begins by defining the wave action spectrum $n_k = \frac{L}{2\pi}\langle|\hat{\psi}_k|^2\rangle$, where the $\langle\cdot\rangle$ denotes an ensemble average (or a time average for statistically stationary data). In deriving the WKE governing n_k, a statistical closure needs to be taken which connects 4th-order correlation of $\hat{\psi}_k$ to n_k, in the form of

$$\mathrm{Im}\langle\hat{\psi}_1\hat{\psi}_2\hat{\psi}_3^*\hat{\psi}_k^*\rangle_\Omega = 4\pi n_1 n_2 n_3 n_k \times \left(\frac{1}{n_k}+\frac{1}{n_3}-\frac{1}{n_1}-\frac{1}{n_2}\right) f(\Omega), \tag{2}$$

where Ω denotes the frequency mismatch of the four wave modes k_1, k_2, k_3, and k. The closure (2) can be derived in various ways, assuming quasi-Gaussian statistics [1], or more recently under the less restrictive assumption of a field with random phases and amplitudes [22–24]. Depending on different methods of derivation, $f(\Omega)$ takes different forms of a broadened delta function, namely a Lorentzian form [25] or sinc-like functions [26,27]. At the kinetic limit, we have $f(\Omega) \to \delta(\Omega)$ and reach the WKE:

$$\frac{\partial n_k}{\partial t} = \iiint 4\pi n_1 n_2 n_3 n_k\left(\frac{1}{n_k}+\frac{1}{n_3}-\frac{1}{n_1}-\frac{1}{n_2}\right) \times \delta(k_1+k_2-k_3-k)\delta(\Omega)dk_1dk_2dk_3. \tag{3}$$

One can further seek stationary solutions to (3) using the so-called Zakharov transformation [25]. Of interest here is the KZ solution associated with a finite energy flux from small to large k, taking the form of $n_k = CP^{1/3}k^{-1}$. Included in Appendix A is a full derivation of the KZ spectrum, including a correction to the previous work [19] leading to a new value of $C = 0.2984$.

III. METHODS OF NUMERICAL STUDY

We simulate (1) with Gaussian forcing and dissipation terms on the right-hand side via the pseudospectral method developed in [7]. The simulated equation takes the form

$$i\frac{\partial \psi}{\partial t} = |\partial_x|^{1/2}\psi + |\psi|^2\psi + F - \nu, \tag{4}$$

where F and ν are defined in spectral domain. The dissipation is given by

$$\nu_k = \begin{cases} 3k^{-4}\times i\hat{\psi}_k & 0 < |k| \leqslant 10 \\ 10^{-14}(k-900)^8\times i\hat{\psi}_k & |k| \geqslant 900 \\ 0 & \text{otherwise.} \end{cases} \tag{5}$$

Forcing is applied only on the interval $10 \leqslant |k| \leqslant 20$, with $F_k \equiv \mathrm{Re}[F_k] + i\mathrm{Im}[F_k]$. For each k, both the real and imaginary components are sampled independently and identically from a zero-mean Gaussian distribution whose standard deviation σ_F determines the effective forcing strength (and the final nonlinear strength of the field). We dissipate at the small scales to drive the system into a steady, out-of-equilibrium state associated with an energy cascade toward large $|k|$. Dissipation is added at the large scale to prevent the accumulation via the inverse wave action cascade. Forcing and dissipation of this type have been widely used in the study of the MMT model (e.g., [9]).

For each simulation, we start from a quiescent field and simulate until a stationary spectrum is reached, with the final nonlinearity level measured by $\varepsilon = H_4/H_2$, where H_2 and H_4 are the linear and nonlinear components of total energy of the unforced and undissipated system (1), respectively, given by [7]:

$$H = H_2 + H_4 = \int \left||\partial_x|^{1/4}\psi\right|^2 dx + \frac{1}{2}\int |\psi|^4 dx. \tag{6}$$

For the remainder of this work, ε will be computed from the average values of H_2 and H_4 measured from statistically stationary time data.

To numerically approximate the kinetic limit, we choose four different forcing strengths resulting in four different final nonlinearity levels ε, and for each forcing strength, we conduct simulations on domain of sizes $L \in [2\pi, 4\pi, 8\pi, 16\pi]$. As L increases from 2π to 16π, the resolution in k space progressively doubles with Δk decreasing from 1 to 1/8, with $k_{\max} = 1024$ kept for all simulations. For a fair comparison between domains of different L, we would like to keep key quantities like the length-averaged Hamiltonian density H, ε, and P approximately constant as L increases, while allowing other quantities to vary. Choosing the parameters of each numerical simulation to achieve this goal turns out to be a nontrivial task. Given the definition of our Fourier series

$$\hat{\psi}_k = \frac{1}{L}\int_0^L \psi\, e^{-ik\cdot x}dx, \tag{7}$$

the spectral amplitude $\hat{\psi}_k$ is normalized such that the length-averaged total action does not depend on L, as can be seen via Parseval's theorem [26],

$$\frac{1}{L}\int_0^L |\psi|^2 dx = \sum_{k\in\Lambda_L^2} |\hat{\psi}_k|^2. \tag{8}$$

The key parameters that control the energy content of our simulations are forcing and dissipation. Thus, we attempt to keep the action injection rate, controlled by the standard deviation of the Gaussian forcing σ_F, and the dissipation rate,

controlled by ν_k, the same across domains of different L at each ε of interest. After a careful scaling analysis, we determine that this is achieved by ν_k remaining constant in L, while $\sigma_F \sim 1/\sqrt{L}$. Under this scheme, we find H, ε, P, and other related quantities remain close to constant as L increases.

With numerical data available, we are interested in studying the behavior of the closure model (2), especially in the context of a large number of quartets forming the energy flux. The basis for this analysis is an exact evaluation and decomposition of energy flux developed in [28]:

$$P(k_b) = \sum_{\Omega} P_\Omega(k_b), \tag{9}$$

$$P_\Omega(k_b) = -\sum_{|k|<k_b} \omega_k \sum_{(k_1,k_2,k_3)\in S_{\Omega,k}} 2\mathrm{Im}\langle \hat{\psi}_1 \hat{\psi}_2 \hat{\psi}_3^* \hat{\psi}_k^* \rangle, \tag{10}$$

where k_b is the wave number through which the time-averaged flux P is evaluated, $S_{\Omega,k} \equiv \{(k_1,k_2,k_3)|\ k_1+k_2-k_3-k=0,\ |\omega_1+\omega_2-\omega_3-\omega_k|=\Omega\}$. Equation (9) describes the decomposition of energy flux into contributions from quartets with the wave number condition satisfied and with a mismatch of Ω in frequency condition. The formulation of P_Ω in (10) can be derived directly from (1) without any assumption [28]. With the closure model (2) substituted in (10), we have

$$P_\Omega(k_b) = -\sum_{\boldsymbol{k}\in\{\boldsymbol{k}||k|<k_b\}} \omega_k \sum_{(k_1,k_2,k_3)\in S_{\Omega,k}} 4\pi n_1 n_2 n_3 n_k \times \left(\frac{1}{n_k}+\frac{1}{n_3}-\frac{1}{n_1}-\frac{1}{n_2}\right) f(\Omega). \tag{11}$$

By computing the left-hand side of (11) through (10) and the right-hand side via n_k taken from our simulation data, we can directly compute the functional form of $f(\Omega)$. Comparison of the numerically resolved $f(\Omega)$ with the analytical function then provides us a metric to evaluate the validity of the closure model. We note that this method evaluates the performance of (2) over a large number of quartets, which is shown in [28] as the only meaningful way to study the closure model with a single simulation. In addition, since the right-hand side of (11) is exactly the energy flux calculated from a discrete form of WKE with a broadened delta function, named quasiresonant WKE (QRWKE) in [14], the closeness between numerical and analytical $f(\Omega)$ also indicates the accuracy of the WKE (or QRWKE) in reproducing the energy flux in dynamical simulations.

Finally, before we present our results in full, we remark that we have ensured that the averaged quantities we compute from long time series are convergent. That is, averaging over additional time data does not meaningfully change the values we obtain. Some of the distributions we sample, as we will show, have a relatively large standard deviation, meaning that a large amount of data is needed to accurately compute these statistics. Those few measurements where uncertainty is non-negligible will be indicated. A full exposition and discussion of the deviations and higher moments of the field, however, is outside the scope of this work.

IV. RESULTS

We begin by showing in Fig. 1 the stationary spectra for all 16 simulations varying nonlinearity level $\varepsilon \in (0.0066, 0.067)$

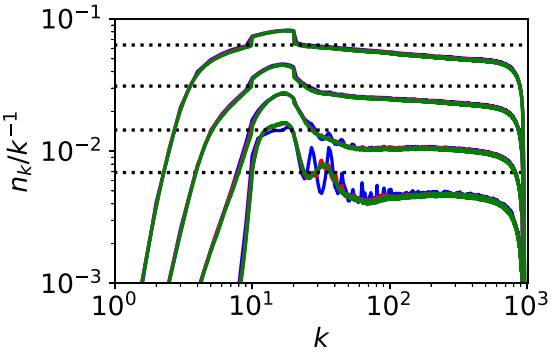

FIG. 1. The directionally averaged compensated wave action spectra n_k/k^{-1} for each tested case. Colors denote $L = 2\pi$ (blue), $L = 4\pi$ (red), $L = 8\pi$ (magenta), and $L = 16\pi$ (green). The four distinct spectral levels denote the four values of ε. The KZ spectrum associated with $P(k_b = 300)$ from the $L = 16\pi$ case at each ε is also plotted (dotted lines).

and domain size L. At high nonlinearity levels, we see good agreement in spectral form for all L, indicating that even the smallest domain size $L = 2\pi$ is sufficient to capture the large-L dynamics. At low nonlinearity (especially $\varepsilon = 0.0066$), however, we see that the spectrum varies substantially as L changes. In particular, the secondary peaks occurring at small L reflect finite-size effects. They disappear as L increases, suggesting a transition from the discrete to the kinetic turbulence regime [8,29].

Also shown in Fig. 1 are the KZ solutions, with P computed though $k_b = 300$ for $L = 16\pi$ for each ε. While we see that the spectral slope gets closer to the KZ value of $\gamma = -1$ as as ε decreases, the inertial interval also shrinks, and perhaps even departs slightly from a true power law. Additionally, the spectral level of the numerical solution does not get closer to the KZ solution as nonlinearity is decreased, indicating that the numerically resolved Kolmogorov constant does not agree better with its theoretical value. We note that this is not in contradiction with the major theme of the paper. As discussed below, we need to consider two limiting processes to precisely reproduce the theoretical value of C: one taking the kinetic limit, and the other increasing the width of the inertial range.

Before discussing the two limiting processes in detail, we would like to mention another set of important results that are made available by our detailed analysis. Measurement of the long-time trajectory of the field enables resolution of interscale energy flux and high-wave-number dissipation rate probability density functions. We begin with measurements of interscale energy flux $P(k_b = 300, t)$, defined as

$$P(k_b, t) = \sum_{|k|<k_b} \omega_k \frac{d|\hat{\psi}_k|^2}{dt}, \tag{12}$$

where the derivative on the right-hand side may be computed from (1) in its spectral form given some statistically stationary field $\hat{\psi}_k(t)$. Results only for the highest nonlinearity case are shown in Fig. 2(a); however they are representative of the other cases. $P(t)$ takes a Gaussian distribution whose standard deviation is much larger than its mean.

This is a similar result to our previous work in a 2D MMT model with a nonlinear Schrödinger equation–like dispersion

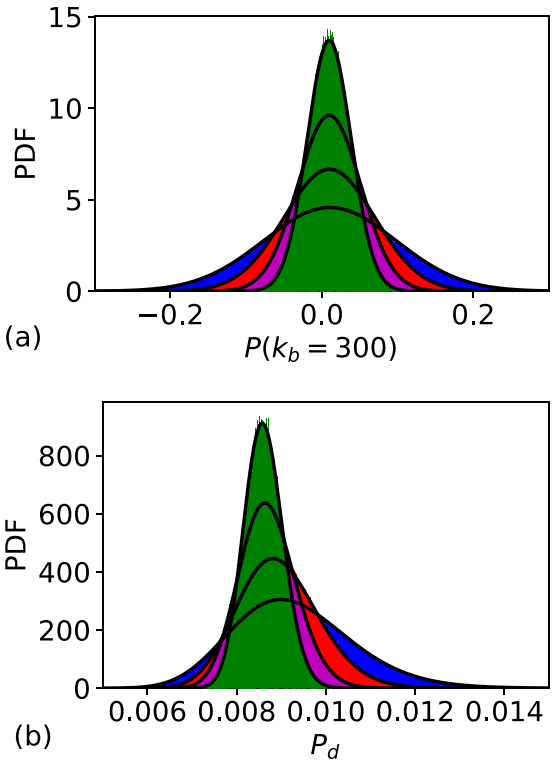

FIG. 2. The distributions of $P(k_b, t)$ (a) and $P_d(t)$ (b) for the highest ε data, for $L = 2\pi$ (blue), $L = 2\pi$ (red), $L = 2\pi$ (magenta), and $L = 2\pi$ (green). The distributions given by the solid curves represent Gaussian (a) and log-normal (b) distributions of equal mean and variance to the data they outline.

relation [28], suggesting a Gaussian energy cascade is a general feature of wave turbulence. In fact, a simple argument supports a Gaussian energy cascade: first, consider the form of (12), which expresses the instantaneous interscale flux as a sum over a large number of modes. If the the instantaneous time rate of change of energy at each of these modes is assumed to be independent, then the central limit theorem (CLT) can be used to show that $P(k_b, t)$ approaches a Gaussian distribution as the number of modes in the domain becomes large. Similar arguments can be used in conjunction with (1) and (8) to derive the observed scaling of the standard deviation $\sigma(P(k_b, t)) \sim 1/\sqrt{L}$.

In Fig. 2(b), we provide the steady time distribution of high wave number dissipation rate, derived directly from the dissipation term to be

$$P_d(t) \equiv -\sum_{|k|>900} 2\omega_k \nu_k |\hat{\psi}_k|^2. \tag{13}$$

The distribution is log-normal, and the standard deviation exhibits the same $1/\sqrt{L}$ scaling due to similar arguments. Log-normal distributions of dissipation rate have been described in flow turbulence [30,31]; however we are not aware of similar results in WT. Now, we proceed to our discussion of the kinetic limit.

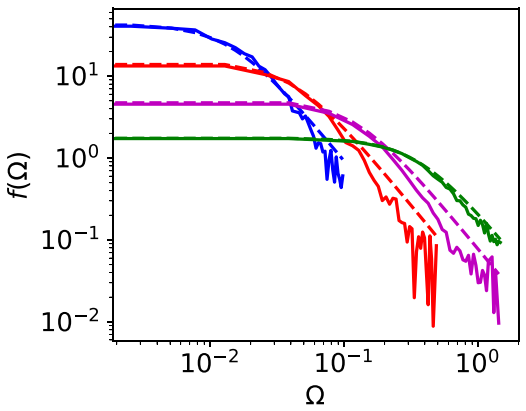

FIG. 3. The measured closure function $f(\Omega)$ (solid curves) for each tested $L = 16\pi$ case, denoted from highest to lowest ε by green, magenta, red, and blue, respectively. A fitted Lorentzian closure $f(\Omega)$ for each case (dashed curves). The fluctuations seen for large Ω are due to uncertainty in the measurement of the mean of high-variance data. Measurements of $f(\Omega)$ for small Ω, which determines the bulk of the dynamics, are fully converged.

A. Limiting process 1: Kinetic limit

In this section, we will show that as the kinetic limit is taken, the measured energy flux indeed converges to the prediction of the WKE. Following methods introduced in Sec. III, we plot $f(\Omega)$ for different nonlinearity levels at $L = 16\pi$, together with the analytical Lorentzian form $a/\pi(a^2 + \Omega^2)$ [25] with values of a that best fit the data, in Fig. 3. We see that the analytical form fits the data remarkably well, and that as nonlinearity is decreased with sufficient domain size, the function $f(\Omega)$ approaches a true delta function. These results indicate that the long-time dynamics indeed follow the WT closure and converge to the WKE description as the kinetic limit is taken. Due to the broadening of $f(\Omega)$, these results also suggest that dynamics away from the kinetic limit may be better represented by the QRWKE. Since the Lorentzian form of the delta functions contains long tails, it is expected that a large number of quasiresonances are active in dynamic simulations away from the kinetic limit. These quasiresonances are therefore key factors resulting in difference in energy flux from dynamical simulations and WKE calculations as seen in [16].

B. Limiting process 2: Wide inertial range

The convergence of dynamics to the WKE prediction at the kinetic limit does not guarantee that the simulated spectrum converges to the KZ solution, as we have demonstrated. As a result, the Kolmogorov constants evaluated for the simulated spectrum using the dynamic flux (10) and kinetic flux (11) with $f(\Omega) \to \delta(\Omega)$ are very close to each other but are far away from the theoretical value [see symbols in Fig. 4(b)]. To understand this situation, recall that, given a valid WKE, the realization of the KZ solution requires the dominance of local interactions, which in turn requires a sufficiently wide inertial range. The width of inertial range seems to be especially important for 1D models such as MMT, as evidenced in [9] on the sensitivity of γ to the width. It is our objective

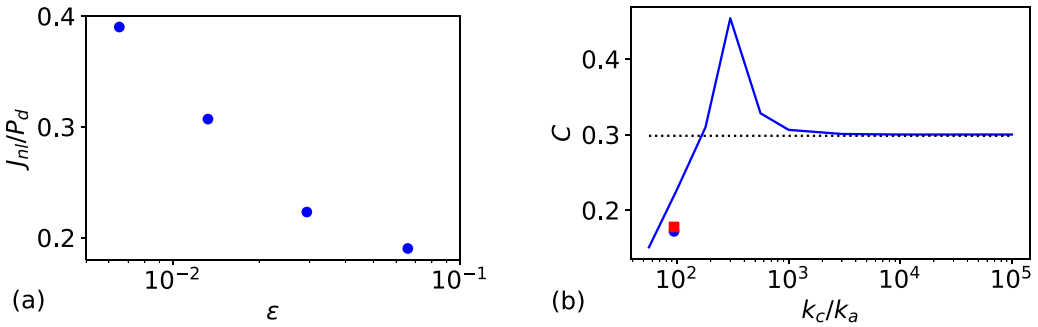

FIG. 4. (a) The relative contribution of (nonlocal) interactions with the forcing range to the average small-scale dissipation rate for varying ε, plotted for the (representative) $L = 16\pi$ case. (b) Value of C for varying inertial interval length k_c/k_a. Filled square denotes C computed via the kinetic flux for the simulated spectrum. Filled circles denote C computed via dynamic flux for the simulated spectrum.

to show next that our numerical solution is indeed contaminated by nonlocal interactions, and that a much wider inertial range is needed to precisely recover the theoretical value of C.

We first quantify the influence of the forcing-range spectral peak (as the source of non-local interactions) on the high-wave-number portion of the spectrum. Considering the stationary state, we explicitly decompose the average small-scale dissipation rate via $P_d = J_{nl} + J_l$, where J is the small-scale energy evolution due to nonlinear interactions with subscripts nl and l denoting contributions from nonlocal and local interactions, respectively. An interaction is considered nonlocal if at least one wave number resides in the forcing range ($10 \leqslant |k| \leqslant 20$). To compute these nonlocal contributions directly from our numerical data in an efficient way, we refine methods developed in [32]. The full technique is presented in Appendix C, and the resulting ratio J_{nl}/P_d is depicted in Fig. 4(a). At low nonlinearities, about 40% of the interscale energy flux is due to nonlocal interactions, clearly violating the assumptions of the KZ spectrum. Interestingly, the nonlocal contribution decreases as nonlinearity is increased, explaining the longer power-law range at higher nonlinearity seen in Fig. 1.

We finally demonstrate precise convergence to the theoretical value of C as the width of inertial range is made larger. This is achieved by evaluating kinetic flux P_{WKE} for an idealized spectrum $n_k = k^{-1}$ with cutoffs at both low and high wave numbers k_a and k_c. Here $P_{WKE} \equiv \int_{k_a}^{k_b} \omega_k \partial n_k/\partial t$ with $\partial n_k/\partial t$ computed from the collision integral of the WKE (3), which is exactly the right-hand side of (11) with $f(\Omega) \to \delta(\Omega)$. Details on our method for evaluation of the collision integral are available in Appendix B. Specifically, we keep $k_a = 10$ and progressively move k_c to a higher wave number to represent the widening of the inertial range, with P_{WKE} evaluated at $k_b = 560$. Figure 4(b) plots the value of C as a function of k_c/k_a. At $k_c/k_a \approx 100$, some discrepancy is seen between C evaluated on the simulated and idealized spectra, due the differences in form between the two spectra. With the increase of k_c/k_a, we see that the value of C converges to the theoretical value with very high precision. We find that an inertial range of about 3.5 decades is needed to obtain converged and accurate result for C. This is much longer than what is needed to recover the theoretical γ in the MMT model [9] and what is needed for C in high-dimensional models [16].

In addition, we note that for the MMT model we consider, $\gamma = -1$ is far from the boundaries of the locality window $-7/4 < \gamma < 1/2$ [19]. The long inertial range needed to recover the KZ solution is therefore more likely a general feature of the 1D wave turbulence. We also comment that recent theoretical work [33] demonstrates that higher-order corrections to the WKE lead to ultraviolet divergences for the KZ spectra. Our conclusion that the KZ spectrum is recovered for a very long inertial interval is not a contradiction to this theoretical development as we have considered the WKE only up to leading order.

V. CONCLUSION

We present a detailed numerical study on the MMT model, focusing on the realization of the Kolmogorov constant and the WT closure. We show that the Kolmogorov constant can be precisely recovered following two limiting processes: the first as the kinetic limit is taken where the dynamics converges to the WKE prediction in terms of the WT closure model realized through energy flux; the second as the inertial-range spectrum is made sufficiently wide so that enough interactions over the inertial range are captured.

ACKNOWLEDGMENTS

We thank Zaher Hani, Sergey Nazarenko, and Peter Miller for their thoughtful comments and suggestions. This work was supported by a grant from the Simons Foundation (Award No. 651459, Y.P.). This material is also based on work supported by the National Science Foundation Graduate Research Fellowship under Grant No. DGE 1841052 (A.H.). This work additionally used Bridges-2 at Pittsburgh Supercomputing Center through Allocation No. phy220053p from the Advanced Cyberinfrastructure Coordination Ecosystem: Services and Support (ACCESS) program, which is supported by National Science Foundation Grants No. 2138259, No. 2138286, No. 2138307, No. 2137603, and No. 2138296.

Any opinions, findings, and conclusions or recommendations expressed in this material are those of the authors and do not necessarily reflect the views of the National Science Foundation.

APPENDIX A: DERIVATION OF THE KOLMOGOROV-ZAKHAROV SPECTRUM

The derivation of the KZ spectrum begins with the wave kinetic equation (WKE) (3). While it is not in general necessary [26], we adopt the popular assumption of an isotropic spectrum. In one-dimensional systems, this takes the form of $n_k = n_{-k}$. Each of k_1, k_2, and k_3 can take a positive or negative sign in the delta function of (3), producing 8 possibilities. However, not every combination of these signs produces a nontrivial resonance. A trivial resonance is one that satisfies the resonance conditions by having $k_1 = k_3$ and $k_2 = k$, or $k_2 = k_3$ and $k_1 = k$. For these cases, the integrand of (3) takes a zero value, so they may be ignored. After these trivial cases are removed, we are left with

$$\begin{aligned}\frac{\partial n_k}{\partial t} =& 4\pi \int_0^\infty \int_0^\infty \int_0^\infty n_1 n_2 n_3 n_k \left(\frac{1}{n_k} + \frac{1}{n_3} - \frac{1}{n_1} - \frac{1}{n_2}\right) \\ &\times \delta(\omega_1 + \omega_2 - \omega_3 - \omega_k)[\delta(k_1 + k_2 + k_3 - k) + \\ &\times \delta(k_1 - k_2 - k_3 - k) + \delta(-k_1 + k_2 - k_3 - k) \\ &+ \delta(-k_1 - k_2 + k_3 - k)]dk_1 dk_2 dk_3. \end{aligned} \tag{A1}$$

It will later become important to integrate over the resonant manifold (described by the δ functions), which is much easier to interpret as quadratic functions in $\omega = k^{1/2}$. Therefore, we next rewrite the above equation as an integral over ω, and replace (on the left-hand side) n_k, the spectral density in k, with $\mathcal{N}_\omega$, the spectral density in ω. This leads to

$$\begin{aligned}\frac{\partial \mathcal{N}_\omega}{\partial t} =& 128\pi \int_0^\infty \int_0^\infty \int_0^\infty (\omega_1\omega_2\omega_3\omega) n_1 n_2 n_3 n_\omega \\ &\times \left(\frac{1}{n_\omega} + \frac{1}{n_3} - \frac{1}{n_1} - \frac{1}{n_2}\right)\delta(\omega_1 + \omega_2 - \omega_3 - \omega) \\ &\times \left[\delta\left(\omega_1^2 + \omega_2^2 + \omega_3^2 - \omega^2\right) + \delta\left(\omega_1^2 - \omega_2^2 - \omega_3^2 - \omega^2\right)\right. \\ &+ \delta\left(-\omega_1^2 + \omega_2^2 - \omega_3^2 - \omega^2\right) \\ &\left.+ \delta\left(-\omega_1^2 - \omega_2^2 + \omega_3^2 - \omega^2\right)\right] \\ &\times d\omega_1 d\omega_2 d\omega_3, \end{aligned} \tag{A2}$$

where $n_\omega = n(k(\omega))$, and we have used the facts that $dk = 2\omega d\omega$ and $\mathcal{N}(\omega)d\omega = n(k)dk + n(-k)dk = 2n(k)dk$. We note that the factor of 2 on the spectral element relation is necessary for a consistent and correct flux definition.

We now assume that $n_\omega = A\omega^\gamma$, where γ refers to an arbitrary exponent that will later be used to determine the KZ exponents. Substituting this into (A2), we are left with

$$\begin{aligned}\frac{\partial \mathcal{N}_\omega}{\partial t} =& 128\pi A^3 \int_0^\infty \int_0^\infty \int_0^\infty \omega_1^{\gamma+1}\omega_2^{\gamma+1}\omega_3^{\gamma+1}\omega^{\gamma+1} \\ &\times \left(\omega^{-\gamma} + \omega_3^{-\gamma} - \omega_1^{-\gamma} - \omega_2^{-\gamma}\right)\delta(\omega_1 + \omega_2 - \omega_3 - \omega) \\ &\times \left[\delta\left(\omega_1^2 + \omega_2^2 + \omega_3^2 - \omega^2\right) + \delta\left(\omega_1^2 - \omega_2^2 - \omega_3^2 - \omega^2\right)\right. \\ &+ \delta\left(-\omega_1^2 + \omega_2^2 - \omega_3^2 - \omega^2\right) \\ &\left.+ \delta\left(-\omega_1^2 - \omega_2^2 + \omega_3^2 - \omega^2\right)\right] \\ &\times d\omega_1 d\omega_2 d\omega_3. \end{aligned} \tag{A3}$$

Next we employ the Zakharov transformations [25,26], which are a set of conformal transformations one applies to the integrand that result in the reduction of the sum of delta functions to a single delta function. This new structure of the integrand will allow us to (a) explicitly see the zeros of the equation and (b) explicitly compute the Kolmogorov constant C. See [7] for an intuitive, geometric description of how these transformations achieve these effects assuming only a self-similar spectrum. We distribute the sum of delta functions to expand the integrand into 4 terms, and we handle each separately. The first term,

$$\begin{aligned}\frac{\partial \mathcal{N}_\omega}{\partial t}^{(1)} =& 128\pi A^3 \int_0^\infty \int_0^\infty \int_0^\infty \omega_1^{\gamma+1}\omega_2^{\gamma+1}\omega_3^{\gamma+1}\omega^{\gamma+1} \\ &\times \left(\omega^{-\gamma} + \omega_3^{-\gamma} - \omega_1^{-\gamma} - \omega_2^{-\gamma}\right) \\ &\times \delta(\omega_1 + \omega_2 - \omega_3 - \omega) \\ &\times \delta\left(\omega_1^2 + \omega_2^2 + \omega_3^2 - \omega^2\right)d\omega_1 d\omega_2 d\omega_3, \end{aligned} \tag{A4}$$

is the form onto which we will map the other terms. We have used a superscript (1) to denote that we are referring to the first term. Now, as an example, we manipulate the second term in full,

$$\begin{aligned}\frac{\partial \mathcal{N}_\omega}{\partial t}^{(2)} =& 128\pi A^3 \int_0^\infty \int_0^\infty \int_0^\infty \omega_1^{\gamma+1}\omega_2^{\gamma+1}\omega_3^{\gamma+1}\omega^{\gamma+1} \\ &\times \left(\omega^{-\gamma} + \omega_3^{-\gamma} - \omega_1^{-\gamma} - \omega_2^{-\gamma}\right) \\ &\times \delta(\omega_1 + \omega_2 - \omega_3 - \omega) \\ &\times \delta\left(\omega_1^2 - \omega_2^2 - \omega_3^2 - \omega^2\right)d\omega_1 d\omega_2 d\omega_3, \end{aligned} \tag{A5}$$

to which we apply the following transformations: $\omega_1 = \omega^2/\omega_1'$, $\omega_2 = \omega\omega_2'/\omega_1'$, and $\omega_3 = \omega\omega_2'/\omega_1'$. Under these transformations, $d\omega_1 d\omega_2 d\omega_3 = (\frac{\omega}{\omega_1'})^4 d\omega_1' d\omega_2' d\omega_3'$, and (A5) becomes, after some reduction,

$$\begin{aligned}\frac{\partial \mathcal{N}_\omega}{\partial t}^{(2)} =& 128\pi A^3 \int_0^\infty \int_0^\infty \int_0^\infty \left(\frac{\omega}{\omega_1'}\right)^{3\gamma+5} \omega_1'^{\gamma+1}\omega_2'^{\gamma+1}\omega_3'^{\gamma+1}\omega'^{\gamma+1} \\ &\times \left(\omega_1'^{-\gamma} + \omega_3'^{-\gamma} - \omega'^{-\gamma} - \omega_2'^{-\gamma}\right)\delta(\omega' + \omega_2' - \omega_3' - \omega_1') \\ &\times \delta\left(\omega_1'^2 + \omega_2'^2 + \omega_3'^2 - \omega'^2\right)d\omega_1' d\omega_2' d\omega_3'. \end{aligned} \tag{A6}$$

We note that the identity $\int \delta(ax)dx = \int \delta(x)/|a|dx$ is used to simply the above expression. The integrand of (A6) *almost* reflects (A4) with an additional factor of $(\omega/\omega_1')^{3\gamma+5}$. If one carefully looks at the signed terms in the equation, however, it becomes apparent that certain indices have become switched as a result of our transformation. The choice of indices is arbitrary, so we

renumber them according to $123 \to 132$. This leaves us with

$$\frac{\partial \mathcal{N}_\omega}{\partial t}^{(2)} = -128\pi A^3 \int_0^\infty \int_0^\infty \int_0^\infty \left(\frac{\omega}{\omega_1'}\right)^{3\gamma+5} \times \omega_1'^{\gamma+1}\omega_2'^{\gamma+1}\omega_3'^{\gamma+1}\omega'^{\gamma+1}\left(\omega'^{-\gamma}+\omega_3'^{-\gamma}-\omega_1'^{-\gamma}-\omega_2'^{-\gamma}\right) \times \delta(\omega_1'+\omega_2'-\omega_3'-\omega)\delta\left(\omega_1'^2+\omega_2'^2+\omega_3'^2-\omega'^2\right)d\omega_1'd\omega_2'd\omega_3'. \tag{A7}$$

In this form, the symmetry with (A4) is obvious. We perform the remaining Zakharov transformations (see [25] for the forms of the other transformations), sum the four terms, and drop the primes from our notation. This results in

$$\frac{\partial \mathcal{N}_\omega}{\partial t} = 128\pi A^3 \int_0^\infty \int_0^\infty \int_0^\infty \omega_1^{\gamma+1}\omega_2^{\gamma+1}\omega_3^{\gamma+1}\omega^{\gamma+1}\left(\omega^{-\gamma}+\omega_3^{-\gamma}-\omega_1^{-\gamma}-\omega_2^{-\gamma}\right) \times \left[1+\left(\frac{\omega_3}{\omega}\right)^y-\left(\frac{\omega_1}{\omega}\right)^y-\left(\frac{\omega_2}{\omega}\right)^y\right]\delta(\omega_1+\omega_2-\omega_3-\omega) \times \delta\left(\omega_1^2+\omega_2^2+\omega_3^2-\omega^2\right)d\omega_1 d\omega_2 d\omega_3, \tag{A8}$$

with $y \equiv -3\gamma - 5$. Careful consideration of the resonance conditions reveals that (A8) is an integral over the intersection of the plane $\omega_1+\omega_2-\omega_3-\omega=0$ and the sphere $\omega_1^2+\omega_2^2+\omega_3^2=\omega^2$ for any given ω. Thus, we do not need to consider integrating over any $\omega_i > \omega$. This enables a reparametrization in terms of some $\xi_i = \omega_i/\omega \in [0,1]$, so that (A8) becomes

$$\frac{\partial \mathcal{N}_\omega}{\partial t} = 128\pi A^3\omega^{-y-1}I(y) = 128\pi A^3\omega^{-y-1} \times \int_0^1\int_0^1\int_0^1 (\xi_1\xi_2\xi_3)^{\gamma+1}\left(1+\xi_3^{-\gamma}-\xi_1^{-\gamma}-\xi_2^{-\gamma}\right) \times (1+\xi_3^y-\xi_1^y-\xi_2^y)\delta(\xi_1+\xi_2-\xi_3-1) \times \delta\left(\xi_1^2+\xi_2^2+\xi_3^2-1\right)d\xi_1 d\xi_2 d\xi_3. \tag{A9}$$

This is the form of the WKE that allows for the solution of γ corresponding to stationary solutions.

One can see by the second product in the integrand that if $\gamma = 0$, the right-hand side of (A9) is identically 0. This corresponds to equipartition of wave action; i.e., n_ω is constant. Also, if $\gamma = -1$, then the second product is identically 0 whenever the resonance condition is satisfied, also leading to a 0 of the collision integral. This solution $n_\omega = A/\omega$ corresponds to the Rayleigh-Jeans spectrum. Neither of these solutions corresponds to wave turbulence, but rather they are equilibrium solutions. The KZ solutions are given by $y = 0$ and $y = 1$, which produce 0′s of the collision integral by the same arguments as the equilibrium solutions. Setting $y = 0$, one obtains $n_\omega = A\omega^{-5/3}$, and for $y = 1$, one obtains $n_\omega = A\omega^{-2}$. To determine which of these out-of-equilibrium spectra correspond to the forward cascade of energy and which corresponds to the inverse cascade of wave action, one may use the ordering of the exponents γ relative to the equilibrium spectra [26], or Zakharov's method via evaluating (A9) [19], while in both cases being careful to ensure the flux directions are not nonphysical via comparison to the equilibrium spectra [19,25,26]. In [19], it is demonstrated that the forward and inverse cascade for our system have physical cascade directions and that $y = 1$ (with $\gamma = -2$) corresponds to the forward cascade.

Next, we derive the Kolmogorov constant C. The energy flux through frequency ω is defined by a control volume argument in spectral space as

$$P(\omega) \equiv -\int_0^\omega \omega' \frac{\partial \mathcal{N}}{\partial t}(\omega')d\omega' = -128\pi A^3 \frac{\omega^{1-y}}{1-y} I(y), \tag{A10}$$

where a negative sign is introduced to ensure that a positive flux corresponds to a cascade of energy from large to small scales (long to short timescales via the dispersion relation). For the forward cascade with $y = 1$, the computation of $P(\omega)$ involves the limit of an indeterminate quantity, which can be obtained via L'Hospital's rule to be

$$P(\omega) = 128\pi A^3 \lim_{y\to 1}\frac{dI(y)}{dy}. \tag{A11}$$

The limit of the desired derivative, S, is given by

$$S = \lim_{y\to 1}\frac{dI(y)}{dy} = \int_0^1\int_0^1\int_0^1 (\xi_1\xi_2\xi_3)^{-1}\left(1+\xi_3^2-\xi_1^2-\xi_2^2\right) \times (\xi_3\ln\xi_3-\xi_1\ln\xi_1-\xi_2\ln\xi_2)\delta(\xi_1+\xi_2-\xi_3-1) \times \delta\left(\xi_1^2+\xi_2^2+\xi_3^2-1\right)d\xi_1 d\xi_2 d\xi_3, \tag{A12}$$

where we have used the fact that $\lim_{y\to 1}\frac{dx^y}{dy} = x\ln x$. In the next section, we develop a precise method to numerically evaluate (A12) to find $S = 0.09353$. We now compute the relationship between A and $P(\omega)$, revealing the Kolmogorov constant C via

$$A = CP^{1/3} = (128\pi S)^{-1/3}P^{1/3}, \tag{A13}$$

resulting in $C = 0.2984$. Given that C is positive, we can now be sure that the cascade direction is correct. Thus, the KZ spectrum associated with the forward cascade process in our MMT equation is given by $n_\omega = 0.2984P^{1/3}\omega^{-2}$, or, via the linear dispersion relation, $n_k = 0.2984P^{1/3}k^{-1}$. We note that this value of C is different from the result of Zakharov *et al.* [19], due to their missing factor of 2 in the spectral element relation $\mathcal{N}(\omega)d\omega = 2n(k)dk$.

APPENDIX B: NUMERICAL INTEGRATION OVER THE RESONANT MANIFOLD

1. Evaluation of S

We are interested in integrating (A12). For simplicity, we will refer to the non-delta part of the integrand by $f(\xi_1, \xi_2, \xi_3)$ so that

$$f(\xi_1, \xi_2, \xi_3) \equiv (\xi_1\xi_2\xi_3)^{-1}\big(1 + \xi_3^2 - \xi_1^2 - \xi_2^2\big) \times (\xi_3 \ln \xi_3 - \xi_1 \ln \xi_1 - \xi_2 \ln \xi_2). \tag{B1}$$

This leaves

$$S = \int_0^1 \int_0^1 \int_0^1 f(\xi_1, \xi_2, \xi_3)\delta(\xi_1 + \xi_2 - \xi_3 - 1) \times \delta\big(\xi_1^2 + \xi_2^2 + \xi_3^2 - 1\big)d\xi_1 d\xi_2 d\xi_3. \tag{B2}$$

The first of these delta functions is linear in ξ_1. Making use of the property

$$\int_0^1 g(x)\delta(x - a)dx = g(a) \text{ for } 0 \leqslant a \leqslant 1, \tag{B3}$$

we can integrate over ξ_3 to obtain

$$S = \iint_{\Delta(\xi_1,\xi_2)} f(\xi_1, \xi_2, \xi_1 + \xi_2 - 1) \times \delta\big(\xi_1^2 + \xi_2^2 + (\xi_1 + \xi_2 - 1)^2 - 1\big)d\xi_1 d\xi_2. \tag{B4}$$

Integrating over the region $\Delta(\xi_1, \xi_2) \equiv \{0 < \xi_1 < 1, 0 < \xi_2 < 1, 1 < \xi_1 + \xi_2 < 2\}$ simply ensures $0 < \xi_3 < 1$. We would like to now apply (B3) again; however we require a transformation so that the argument $\xi_1^2 + \xi_2^2 + \xi_3^2 - 1$ is of the required form. To do this, we transform the inner integral to one with respect to du, where $u = \xi_1^2 + \xi_2^2 + (\xi_1 + \xi_2 - 1)^2 - 1$ and $du = 2(2\xi_1 + \xi_2 - 1)d\xi_1$. This leaves

$$S = \iint_{\Delta(u,\xi_2)} \frac{f(\xi_1(u), \xi_2, \xi_1(u) + \xi_2 - 1)}{2[2\xi_1(u) + \xi_2 - 1]}\delta(u)du d\xi_2. \tag{B5}$$

Now, we may apply (B3), being careful to include only the part of $u(\xi_1, \xi_2) = 0$ that lies in $\Delta(\xi_1, \xi_2)$. After some manipulation of our definition of u we find that, of the two branches for which $u = 0$, the one with

$$\xi_1 = \frac{1 - \xi_2 + \sqrt{(1 - \xi_2)(3\xi_2 + 1)}}{2}, \quad 0 < \xi_2 < 1, \tag{B6}$$

is in the region $\Delta(\xi_1, \xi_2)$. After applying (B3),

$$S = \int_0^1 \frac{f(\xi_1(\xi_2), \xi_2, \xi_1(\xi_2) + \xi_2 - 1)}{2\sqrt{(1 - \xi_2)(3\xi_2 + 1)}}d\xi_2. \tag{B7}$$

This form of S is suitable for numerical integration, where the integrand as $\xi_2 \to 1$ (from below) can be shown to approach zero via L'Hospital's rule.

2. Evaluation of the WKE collision integral

Just as in the evaluation of $\frac{dI(y)}{dy}$, this explicit algebraic approach works to evaluate (A2). To start, we rewrite (A2) in terms of the function $f(\omega_1, \omega_2, \omega_3, \omega) = \omega_1\omega_2\omega_3\omega n_1 n_2 n_3 n_\omega(\frac{1}{n_\omega} + \frac{1}{n_3} - \frac{1}{n_1} - \frac{1}{n_2})$:

$$\frac{\partial \mathcal{N}_\omega}{\partial t} = 128\pi \int_0^\infty \int_0^\infty \int_0^\infty f(\omega_1, \omega_2, \omega_3, \omega)\big[\delta\big(\omega_1^2 + \omega_2^2 + \omega_3^2 - \omega^2\big) + \delta\big(\omega_1^2 - \omega_2^2 - \omega_3^2 - \omega^2\big) + \delta\big(-\omega_1^2 + \omega_2^2 - \omega_3^2 - \omega^2\big) + \delta\big(-\omega_1^2 - \omega_2^2 + \omega_3^2 - \omega^2\big)\big]d\omega_1 d\omega_2 d\omega_3. \tag{B8}$$

For each δ function with quadratic arguments in ω, we perform the procedure outlined in the previous subsection. After a good deal of simplification, this results in the expression for $\frac{\partial \mathcal{N}_\omega}{\partial t}$ given by Eqs. (B9)–(B14):

$$\frac{\partial \mathcal{N}_\omega}{\partial t} = \frac{\partial \mathcal{N}_\omega^{(1a)}}{\partial t} + \frac{\partial \mathcal{N}_\omega^{(1b)}}{\partial t} + \frac{\partial \mathcal{N}_\omega^{(2)}}{\partial t} + \frac{\partial \mathcal{N}_\omega^{(3a)}}{\partial t} + \frac{\partial \mathcal{N}_\omega^{(3b)}}{\partial t}, \text{ where} \tag{B9}$$

$$\frac{\partial \mathcal{N}_\omega^{(1a)}}{\partial t} = \int_0^{\sqrt{4/3}\omega} \frac{f(\omega_1^{(1a)}(u), \omega_2^{(1a)}(u), \omega_3^{(1a)}(u), \omega)}{2\sqrt{4\omega^2 - 3u^2}}du, \tag{B10}$$

$$\frac{\partial \mathcal{N}_\omega^{(1b)}}{\partial t} = \int_\omega^{\sqrt{4/3}\omega} \frac{f(\omega_1^{(1b)}(u), \omega_2^{(1b)}(u), \omega_3^{(1b)}(u), \omega)}{2\sqrt{4\omega^2 - 3u^2}}du, \tag{B11}$$

$$\frac{\partial \mathcal{N}_\omega^{(2)}}{\partial t} = 2\int_0^\infty \frac{f(\omega_1^{(2)}(u), \omega_2^{(2)}(u), \omega_3^{(2)}(u), \omega)}{2\sqrt{u^2 + 4\omega^2}}du, \tag{B12}$$

$$\frac{\partial \mathcal{N}_\omega^{(3a)}}{\partial t} = \int_0^\infty \frac{f(\omega_1^{(3a)}(u), \omega_2^{(3a)}(u), \omega_3^{(3a)}(u), \omega)}{2\sqrt{u^2 + 4\omega^2}}du, \tag{B13}$$

$$\frac{\partial \mathcal{N}_\omega^{(3b)}}{\partial t} = \int_0^\infty \frac{f(\omega_1^{(3b)}(u), \omega_2^{(3b)}(u), \omega_3^{(3b)}(u), \omega)}{2\sqrt{u^2 + 4\omega^2}}du. \tag{B14}$$

$$(1a)\begin{cases} \omega_2(u) = \frac{1}{3}(\omega + \sqrt{4\omega^2 - 3u^2}), \\ \omega_1(u) = \frac{1}{2}(\omega - \omega_2(u) + \sqrt{[\omega - \omega_2(u)][3\omega_2(u) + \omega]}), \\ \omega_3(u) = \omega_1(u) + \omega_2(u) - \omega, \end{cases} \tag{B15}$$

$$(1b)\begin{cases}\omega_2(u) = \frac{1}{3}(\omega - \sqrt{4\omega^2 - 3u^2}),\\ \omega_1(u) = \frac{1}{2}(\omega - \omega_2(u) + \sqrt{[\omega - \omega_2(u)][3\omega_2(u) + \omega]}),\\ \omega_3(u) = \omega_1(u) + \omega_2(u) - \omega,\end{cases} \tag{B16}$$

$$(2)\begin{cases}\omega_2(u) = -\omega + \sqrt{u^2 + 4\omega^2},\\ \omega_1(u) = \frac{1}{2}(\omega - \omega_2 + \sqrt{[3\omega + \omega_2(u)][\omega_2(u) - \omega]}),\\ \omega_3(u) = \omega_1(u) + \omega_2(u) - \omega,\end{cases} \tag{B17}$$

$$(3a)\begin{cases}\omega_3(u) = \omega + \sqrt{u^2 + 4\omega^2},\\ \omega_2(u) = \frac{1}{2}(\omega + \omega_3(u) + \sqrt{[\omega_3(u) + \omega][\omega_3(u) - 3\omega]}),\\ \omega_1(u) = \omega_3(u) + \omega - \omega_2(u),\end{cases} \tag{B18}$$

$$(3b)\begin{cases}\omega_3(u) = \omega + \sqrt{u^2 + 4\omega^2},\\ \omega_2(u) = \frac{1}{2}(\omega + \omega_3(u) - \sqrt{[\omega_3(u) + \omega][\omega_3(u) - 3\omega]}),\\ \omega_1(u) = \omega_3(u) + \omega - \omega_2(u).\end{cases} \tag{B19}$$

The first delta function on the right-hand side of (B8) corresponds to $\partial\mathcal{N}_\omega^{(1)}/\partial t$, the next two delta functions (due to symmetry) produce identical contributions and are combined in $\partial\mathcal{N}_\omega^{(2)}/\partial t$, and the last delta function corresponds to $\partial\mathcal{N}_\omega^{(3)}/\partial t$. The separate a and b contributions result from multiple branches of the resonant manifold parametrized by u. The corresponding functions of $\omega_i^j(u)$ are given by Eqs. (B15)–(B19).

This is a form of the collision integral that is suitable for numerical integration. When computing P_{WKE} directly from the collision integral in the main text, $n_k \equiv n(k(\omega))$ is evaluated explicitly from the idealized, truncated KZ spectrum given by

$$n_k = \begin{cases}k^{-1}, & k_a \leqslant k \leqslant k_c,\\ 0, & \text{otherwise.}\end{cases} \tag{B20}$$

When the simulated spectrum is instead used in this evaluation [for the two points in Fig. 3(b) of the main text], we use piecewise-linear interpolation of the simulated spectrum to evaluate n_k for $k \notin \Lambda_L$. In both of these cases, $n_k = 0$ after some large value of k with a corresponding u, meaning that the upper integral bounds of $\partial\mathcal{N}_\omega^{(3a)}/\partial t$ and $\partial\mathcal{N}_\omega^{(3b)}/\partial t$ in our numerical evaluations can be taken to be finite. All integrals are evaluated via adaptive quadrature.

APPENDIX C: A FAST DIRECT METHOD FOR COMPUTING NONLOCAL INTERACTIONS

To compute the nonlocal contribution to the small-scale energy evolution rate for a stationary spectrum, we begin by using a control volume argument to express the average dissipation rate directly in terms of the nonlinearity of the MMT model. This is achieved by

$$\begin{aligned}P_d = J &= -\sum_{|k|\geqslant 900} 2\omega_k \nu_k \frac{dn_k}{dt}\\ &= -\sum_{|k|\geqslant 900} 2\omega_k \nu_k \sum_{123} 2\mathrm{Im}\langle\hat\psi_1\hat\psi_2\hat\psi_3^*\hat\psi_k^*\rangle\delta_{3k}^{12},\end{aligned} \tag{C1}$$

where $\delta_{3k}^{12} \equiv \delta_K(k_1 + k_2 - k_3 - k)$. We note that for this section (in contrast to the previous section) P_d indicates a time-averaged quantity. To proceed, we would like to compute the spectral evolution at some wave number $k \in \Lambda_L$ to interactions with the set of wave modes that reside in the forcing range. Let us call this set of forced modes $A \subseteq \Lambda_L$. We will consider an interaction to involve A if *one or more* waves in the interaction are part of A. To express this clearly, it is useful to define the following set of 3-wave triples (k_1, k_2, k_3):

$$S_A^{(i)} \equiv \left\{(k_1,k_2,k_3) \mid (k_i \in A) \cup \left(\bigcup_{j\neq i}(k_j \in \Lambda_L)\right)\right\}. \tag{C2}$$

$S_A^{(i)}$ denotes the set of all 3-wave triples where the ith component is part of A and the other two components are explicitly arbitrary. We are now ready to formally define $\frac{dn(k)}{dt}|_A$, the spectral evolution involving interactions with A:

$$\left.\frac{dn_k}{dt}\right|_A \equiv \sum_{(k_1,k_2,k_3)\in S_A^{(1)}\cup S_A^{(2)}\cup S_A^{(3)}} 2\mathrm{Im}\langle\hat\psi_1\hat\psi_2\hat\psi_3^*\hat\psi_k^*\rangle\delta_{3k}^{12}. \tag{C3}$$

When substituted into (C1), we will obtain the average dissipation rate due to interactions with the forcing range. While the definition of $\frac{dn_k}{dt}|_A$ is clear in this form, it is expensive to compute. However, it is possible to rewrite the expression for the spectral evolution due to interactions with A as a carefully constructed series of sums which can be computed much more quickly.

We start by reformulating (C3) in terms of the evolution of $\hat\psi_k$,

$$\left.\frac{\partial n_k}{\partial t}\right|_A = \left\langle \psi_k \left.\frac{\partial\hat\psi_k^*}{\partial t}\right|_A + \hat\psi_k^* \left.\frac{\partial\hat\psi_k}{\partial t}\right|_A\right\rangle, \tag{C4}$$

with

$$i\left.\frac{\partial\hat\psi_k}{\partial t}\right|_A \equiv \omega_k\psi_k + \sum_{(k_1,k_2,k_3)\in S_A^{(1)}\cup S_A^{(2)}\cup S_A^{(3)}} \psi_1\psi_2\hat\psi_3^*\delta_{3k}^{12}. \tag{C5}$$

It follows from set theory that the sum in the nonlinear term of (C5) can be rewritten as

$$\sum_{(k_1,k_2,k_3)\in S_A^{(1)}\cup S_A^{(2)}\cup S_A^{(3)}} = \sum_{(k_1,k_2,k_3)\in\Lambda_L^3} - \sum_{(k_1,k_2,k_3)\in S_{A^C}^{(1)}\cap S_{A^C}^{(2)}\cap S_{A^C}^{(3)}}, \tag{C6}$$

where A^C is the complement to A. The advantage of this form is that sums over $S_A^{(i)}$ and intersections of $S_A^{(i)}$ can be computed quickly via Fourier transforms. To see this clearly, consider the simple term

$$\hat{NL}\left(k, S_A^{(1)}\right) = \sum_{(k_1,k_2,k_3)\in S_A^{(1)}} \hat{\psi}_1\hat{\psi}_2\hat{\psi}_3^*\delta_{3k}^{12}. \tag{C7}$$

We already know that $\hat{NL}(k, \Lambda_L^3)$ [where the sum is taken over $(k_1, k_2, k_3) \in \Lambda_L^3$] is the Fourier domain representation of a quantity that is readily computed in the physical domain, as this is exactly the pseudospectral method used to solve the MMT equation. Let us call the inverse Fourier transform of (C7) $NL(x, S_A^{(1)})$. This can be written as

$$NL\left(x, S_A^{(1)}\right) = \psi\psi^* \sum_{k_1\in A} \hat{\psi}_1 e^{ik_1x}. \tag{C8}$$

However, the last term in the product (C8) is simply the expression of an ideal bandpass filter applied to ψ that admits only those modes in set A, and sets to 0 any mode with $k \notin A$. Let B_A be such a filter, so that

$$NL\left(x, S_A^{(1)}\right) = \psi\psi^* B_A(\psi). \tag{C9}$$

By exactly the same argument, we compute the second sum on the right-hand side of (C6) by first computing

$$NL\left(x, S_A^{(1)} \cap S_{A^C}^{(2)} \cap S_{A^C}^{(3)}\right) = B_{A^C}(\psi)B_{A^C}(\psi)B_{A^C}(\psi^*). \tag{C10}$$

The inverse Fourier transform can then be used to obtain the desired term in the sum (C6). For N the number of modes, this method has $O(N \log N)$ complexity, as opposed to the $O(N^2)$ complexity of computing (C3) directly. The desired quantity $J_{nl} \equiv J_A$ for $A = [20, 30]$ can then be computed, with

$$J_A = -\sum_{|k|\geqslant 900} 2\omega_k \nu_k \left.\frac{dn_k}{dt}\right|_A. \tag{C11}$$

[1] K. Hasselmann, On the non-linear energy transfer in a gravity-wave spectrum Part 1. General theory, J. Fluid Mech. **12**, 481 (1962).

[2] V. E. Zakharov, Stability of periodic waves of finite amplitude on the surface of a deep fluid, J. Appl. Mech. Tech. Phys. **9**, 190 (1972).

[3] Y. V. Lvov, K. L. Polzin, E. G. Tabak, and N. Yokoyama, Oceanic internal-wave field: Theory of scale-invariant spectra, J. Phys. Oceanogr. **40**, 2605 (2010).

[4] Y. Wu and Y. Pan, Energy cascade in the Garrett-Munk spectrum of internal gravity waves, J. Fluid Mech. **975**, A11 (2023).

[5] S. Nazarenko and M. Onorato, Wave turbulence and vortices in Bose-Einstein condensation, Phys. D (Amsterdam, Neth.) **219**, 1 (2006).

[6] S. Galtier and S. V. Nazarenko, Direct evidence of a dual cascade in gravitational wave turbulence, Phys. Rev. Lett. **127**, 131101 (2021).

[7] A. J. Majda, D. W. McLaughlin, and E. G. Tabak, A one-dimensional model for dispersive wave turbulence, J. Nonlinear Sci. **7**, 9 (1997).

[8] Z. Zhang and Y. Pan, Numerical investigation of turbulence of surface gravity waves, J. Fluid Mech. **933**, A58 (2022).

[9] R. S. Dù and O. Bühler, The impact of frequency bandwidth on a one-dimensional model for dispersive wave turbulence, J. Nonlinear Sci. **33**, 81 (2023).

[10] A. O. Korotkevich, Inverse cascade spectrum of gravity waves in the presence of a condensate: A direct numerical simulation, Phys. Rev. Lett. **130**, 264002 (2023).

[11] L. Deike, M. Berhanu, and E. Falcon, Energy flux measurement from the dissipated energy in capillary wave turbulence, Phys. Rev. E **89**, 023003 (2014).

[12] L. Deike, B. Miquel, P. Gutiérrez, T. Jamin, B. Semin, M. Berhanu, E. Falcon, and F. Bonnefoy, Role of the basin boundary conditions in gravity wave turbulence, J. Fluid Mech. **781**, 196 (2015).

[13] Y. Pan and D. K. P. Yue, Direct numerical investigation of turbulence of capillary waves, Phys. Rev. Lett. **113**, 094501 (2014).

[14] Y. Pan and D. K. P. Yue, Understanding discrete capillary-wave turbulence using a quasi-resonant kinetic equation, J. Fluid Mech. **816**, R1 (2017).

[15] Y. Pan, Understanding of weak turbulence of capillary waves, Ph.D. thesis, Massachusetts Institute of Technology, 2017, https://dspace.mit.edu/handle/1721.1/108837.

[16] Y. Zhu, B. Semisalov, G. Krstulovic, and S. Nazarenko, Direct and inverse cascades in turbulent Bose-Einstein condensates, Phys. Rev. Lett. **130**, 133001 (2023).

[17] Y. Zhu, B. Semisalov, G. Krstulovic, and S. Nazarenko, Testing wave turbulence theory for the Gross-Pitaevskii system, Phys. Rev. E **106**, 014205 (2022).

[18] Y. Deng and Z. Hani, Full derivation of the wave kinetic equation, Invent. math. **233**, 543 (2023).

[19] V. Zakharov, F. Dias, and A. Pushkarev, One-dimensional wave turbulence, Phys. Rep. **398**, 1 (2004).

[20] S. Chibbaro, F. De Lillo, and M. Onorato, Weak versus strong wave turbulence in the Majda-McLaughlin-Tabak model, Phys. Rev. Fluids **2**, 052603(R) (2017).

[21] A. Hrabski and Y. Pan, Effect of discrete resonant manifold structure on discrete wave turbulence, Phys. Rev. E **102**, 041101(R) (2020).

[22] Y. Choi, Y. V. Lvov, and S. Nazarenko, Joint statistics of amplitudes and phases in wave turbulence, Phys. D (Amsterdam, Neth.) **201**, 121 (2005).

[23] G. L. Eyink and Y.-K. Shi, Kinetic wave turbulence, Phys. D (Amsterdam, Neth.) **241**, 1487 (2012).

[24] S. Chibbaro, G. Dematteis, and L. Rondoni, 4-wave dynamics in kinetic wave turbulence, Phys. D (Amsterdam, Neth.) **362**, 24 (2018).

[25] V. E. Zakharov, V. S. L'vov, and G. Falkovich, in *Kolmogorov Spectra of Turbulence I*, edited by F. Calogero, B.

Fuchssteiner, G. Rowlands, H. Segur, M. Wadati, and V. E. Zakharov, Springer Series in Nonlinear Dynamics (Springer, Berlin, 1992).

[26] S. Nazarenko, *Wave Turbulence*, Lecture Notes in Physics Vol. 825 (Springer, Berlin, 2011).

[27] M. Onorato and G. Dematteis, A straightforward derivation of the four-wave kinetic equation in action-angle variables, J. Phys. Commun. **4**, 095016 (2020).

[28] A. Hrabski and Y. Pan, On the properties of energy flux in wave turbulence, J. Fluid Mech. **936**, A47 (2022).

[29] V. S. L'vov and S. Nazarenko, Discrete and mesoscopic regimes of finite-size wave turbulence, Phys. Rev. E **82**, 056322 (2010).

[30] B. B. Mandelbrot, Intermittent turbulence in self-similar cascades: Divergence of high moments and dimension of the carrier, J. Fluid Mech. **62**, 331 (1974).

[31] B. Pearson and B. Fox-Kemper, Log-normal turbulence dissipation in global ocean models, Phys. Rev. Lett. **120**, 094501 (2018).

[32] A. Simonis, A. Hrabski, and Y. Pan, On the time scales of spectral evolution of nonlinear waves, J. Fluid Mech. **979**, A33 (2024).

[33] V. Rosenhaus and G. Falkovich, Interaction renormalization and validity of kinetic equations for turbulent states, arXiv:2308.00033.